

# Features of Coatings Obtained by Supersonic Laser Deposition

A.I. Gorunov<sup>1</sup>

Submitted: 20 May 2017 / in revised form: 3 July 2018 / Published online: 30 August 2018  
© ASM International 2018

**Abstract** The three types of coatings that can be deposited by supersonic laser deposition, namely coatings built without the melting of the processed powder particles, coatings built from molten particles and coatings made from molten particles and with solid particles embedded in the coating, are discussed. For instance, with no melting of the powder material, a titanium alloy coating without transformation of the structure and with a uniform distribution of the chemical elements in the coating cross-section was obtained. Self-fluxing coatings (NiCrCBSiFe) with high hardness were achieved by melting the powder and mixing it with the substrate. The mixing of the coating metal with the substrate metal led to a significant increase in the concentration of the main alloying elements in the coating–substrate interface. X-ray diffraction analysis also showed that the mixing of the NiCrCBSiFe coating with a medium-carbon steel substrate led to the formation of new Fe<sub>x</sub>Ni phases, while their concentration decreased through coating thickness.

**Keywords** chemical composition · microstructure · nickel alloy coating · supersonic laser deposition · titanium alloy

## Introduction

Supersonic laser deposition (SLD) was developed on the basis of the cold spray technique which emerged in the 1980s at the Siberian Branch of the Russian Academy of

Science as a result of research carried out by Professor Alkhimov et al. (Ref 1), who studied the motion of particles in supersonic flows. This method was further developed by Professor O’Neill and the Cambridge University team (Ref 2–4). Later, the spray system was equipped with a laser which increased the productivity of the coating technology and expanded the range of substrate and powder materials. The ability of SLD to deposit Stellite 6 coatings was demonstrated. Later in the work, these results were confirmed (Ref 5).

In recent years, structural characteristics and mechanical properties of titanium alloys obtained by the methods of laser cladding (LC), direct laser deposition of material (Ref 6) and by cold spraying (Ref 7) have been widely investigated.

Usually, either a soft substrate, for example, aluminum, or soft alloys are used as the sprayed material. The possibility of titanium alloy coatings on a steel substrate by supersonic laser deposition has been reported (Ref 8–11). However, the formation of solid wear-resistant coatings from NiCrCBSiFe system materials by supersonic laser deposition has been poorly studied.

The application difficulty of these coatings is related to the fact that their formation requires an increase in the particles’ kinetic energy by raising the temperature at the steel substrate surface or increasing it by another method. As is well known, materials of NiCrCBSiFe system can have a melting temperature 1.5 times lower than the melting temperature of medium carbon steel used as a substrate. High feed velocity of the particles can lead to melting and spattering of the coating metal.

Today, issues related to the deposition of coatings with high hardness on carbon steel substrates by supersonic laser deposition have been poorly investigated, but there are several works devoted to the study of these coatings

✉ A.I. Gorunov  
gorunow.andrej@yandex.ru

<sup>1</sup> Kazan National Research Technical University Named After A.N. Tupolev–KAI, Kazan, Russia 420111

obtained by a laser-cladding method (Ref 12–15). In this context, the paper attempts to go beyond the traditional idea of the coatings produced by cold spraying.

In the research carried out by Bala et al. (Ref 16), NiCr, NiCrTiC, and NiCrTiCRe were deposited by the cold spray technique on SA 516 steel. As a result, the cold-sprayed composite coating of NiCrTiCRe provided maximum erosion–corrosion resistance, with the studies being conducted in an actual boiler environment, which probably contributed the higher hardness and the continuous presence of a protective Cr<sub>2</sub>O<sub>3</sub> layer. In a previous publication (Ref 17), the authors described how Ti6Al4V coatings were deposited on Ti6Al4V substrates using a high-pressure cold spray system. The apparent phase change was not found in the cold-sprayed Ti6Al4V coatings with reference to the Ti6Al4V raw powder. Singh et al. (Ref 18) demonstrated that it is possible to use the cold spray of Inconel 718 powder on an Inconel 718 substrate using nitrogen gas for a repair application of aero engine components. The substrate roughness affected the deposition efficiency and also significantly affected the deformation behavior of the particles on impact with the substrate. The interaction of individual powder particles with different substrate surfaces showed that the localized plastic deformation and interfacial mixing of materials are smaller for substrates with a lower roughness. Ref (19) demonstrates the influence of laser power on the characteristics of Ni60-WC composite coatings deposited using SLD, and compares the results with those deposited using LC. The hardness of the SLD coating is higher compared to that of the LC coating, and its friction coefficient and weight loss are lower. In the considered works, it has been shown that coatings obtained by the SLD method have a number of limitations related to the production of hard coatings. As a rule, the authors used soft powder materials with the addition of hard wear-resistant particles to obtain this result (Ref 20–25). The coatings are formed without melting the powder material, which allows the maintaining of the phase composition and the structure of the original powder material (Ref 26, 27). However, good adhesion of the coating with the substrate surface is not achieved when the deposited metal and the substrate surface are not mixed. Therefore, in this paper, it was decided to combine the LC and SLD methods to partially mix the coating with the substrate and preserve the original powder structure in the coating by the introduction of particles.

The main objective of this investigation was to show the possibilities of the SLD method for obtaining a coating with low and high hardness on a steel substrate without melting the original powder particles. The main methods of supersonic laser deposition of coatings are considered together with new methods of TA15-based and wear-resistant solid NiCrCBSiFe-based coatings deposition.

## Experimental Setup

A schematic diagram of the experimental setup for supersonic laser deposition is shown in Fig. 1.

High-pressure gas is fed to a de Laval nozzle via a heater. Simultaneously the powder material is fed into the nozzle. It is mixed with a heated gas, and the resulting gas–powder mixture is at the same time accelerated to a supersonic speed due to the specific geometry of the nozzle. The substrate surface is under the action of the laser.

The SLD process takes place at a constant temperature controlled by a high speed IR-Pyrometer, and the laser power is periodically adjusted by an automatic control system. The pyrometer determines the temperature of the surface using its emissivity value. Where possible, reference values of the emissivity were used, but sometimes they were not available. Additionally, the pyrometer measurements are sensitive to the surface roughness. Therefore, this approach provides a possibility to determine relative values of the surface temperature, which are suitable for comparison. However, the absolute values of the temperature may be inaccurate so a PID regulator was used. The pyrometer controls the temperature in the contact point, while the PID regulator obtains the pyrometer signal and adjusts the laser power so that the stable conditions in the deposition zone are maintained.

The supersonic nozzle, the laser head, and the pyrometer are fixed: they are static during deposition, and the substrate is moved around by a robot. One of the main features of the unit is the possibility to change the laser head inclination angle, as well as to shift the focus of the laser spot relative to the powder spot.

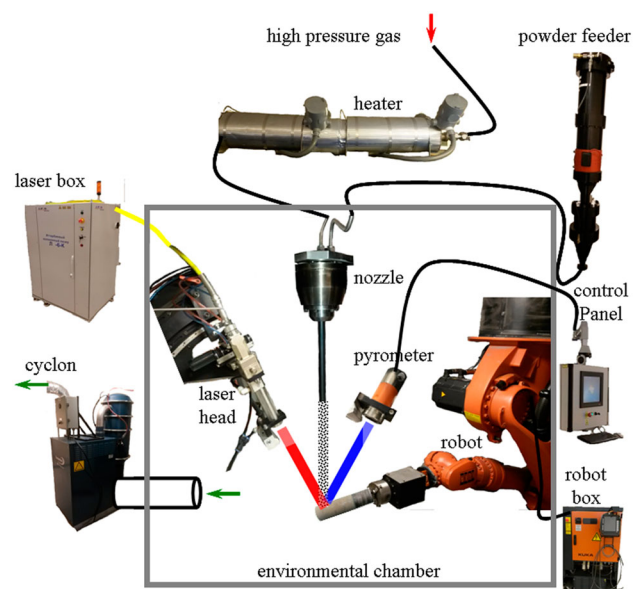


**Fig. 1** Schematic for supersonic laser deposition

**Table 1** Chemical composition of the powder, wt.%

	Al	Mo	V	Zr	O	Ti	Ni	C	Si	B	Fe	Cr	Mn
TA15	6.81	1.1	2.21	2.02	0.14	Bal.							
NiCrCBSiFe	...	...	...	...	...	...	Bal.	0.75	4.3	3.1	3.7	14.8	...
Substrate	...	...	...	...	...	...	0.25	0.4	0.3	...	Bal.	0.25	0.7

**Table 2** Properties of the materials

	HV0.1	T <sub>melt</sub> , °C
TA15	350	1650
NiCrCBSiFe	790	1100
Substrate	460	1500

Two types of spherical powders with diameters ranging between 10 and 50  $\mu\text{m}$  were used in the study. The chemical composition of the powders and substrate in the study are shown in Table 1. Samples were ground step by step by a set of diamond grinding discs (120, 220 and 500 grit) and polished using diamond suspensions (9 and 3  $\mu\text{m}$ ) before analysis. The properties of the both powders and substrate are presented in Table 2.

The powder coating was applied onto a steel-40 cylinder with a diameter of 25 mm and a length of 250 mm by laser-intensified gas-dynamic spraying. The NiCrCBSiFe powder produced by Hoganas and TA15 powder produced by Advanced Powders and Coatings (AP and C) with particles of 50–150  $\mu\text{m}$  were used for the spraying; the ratio of the 100- $\mu\text{m}$  fraction was 18%.

The coating was applied using the IPG Photonics Supersonic Cladding System (Fig. 1). Its operating principle is as follows. Nitrogen at a pressure of 1–3 MPa is divided into two streams. One of the streams is fed into the pre-chamber of the supersonic nozzle; the second one is fed into the supplying powder material. In the supply feeder, the two streams are mixed, and then the gas–powder flow is fed into the nozzle, where it is accelerated to supersonic speed. The jet of the gas–powder mixture and the beam of an IPG Photonics fiber laser with a wavelength of 1070 nm and a maximum power of 6 kW simultaneously act on the substrate. The distance from the substrate surface to the nozzle edge is 40 mm. The optimal process parameters to obtain a single layer of the coating are: nitrogen pressure 3 MPa; nitrogen temperature 550 °C, and laser power 2 kW; the laser beam scanning speed relative to the substrate is 30 mm/s; the powder flow rate 15 g/min; the temperature in the contact spot 1000 °C; and the laser spot diameter 6 mm. Under such conditions, a single layer of metal is deposited in 20 s. After each round of deposition, the samples were held at room temperature until completely cool.

Metallographic analysis of the surface structure of the samples was carried out using an Axio Observer Z1m universal inverted microscope. Electron microscopic images of the surface and the distribution of the chemical elements in the coating were obtained on an Auriga Crossbeam workstation. An automated macro-/micro-durometer Tukon 2500 was used for the microhardness measurements.

X-ray diffraction analysis was carried out using a Rigaku SmartLab multifunctional diffractometer. Diffraction patterns were registered in Bragg–Brentano geometry under the following conditions: 5 mm, 0.25° (divergence slit) slits in the primary beam; 0.3 mm, 0.25° (anti-scatter slit) slits in the diffracted beam; 25–90° scanning interval; 0.02° scanning pitch; and 3.5 s shooting time at the point.

## Results and Discussion

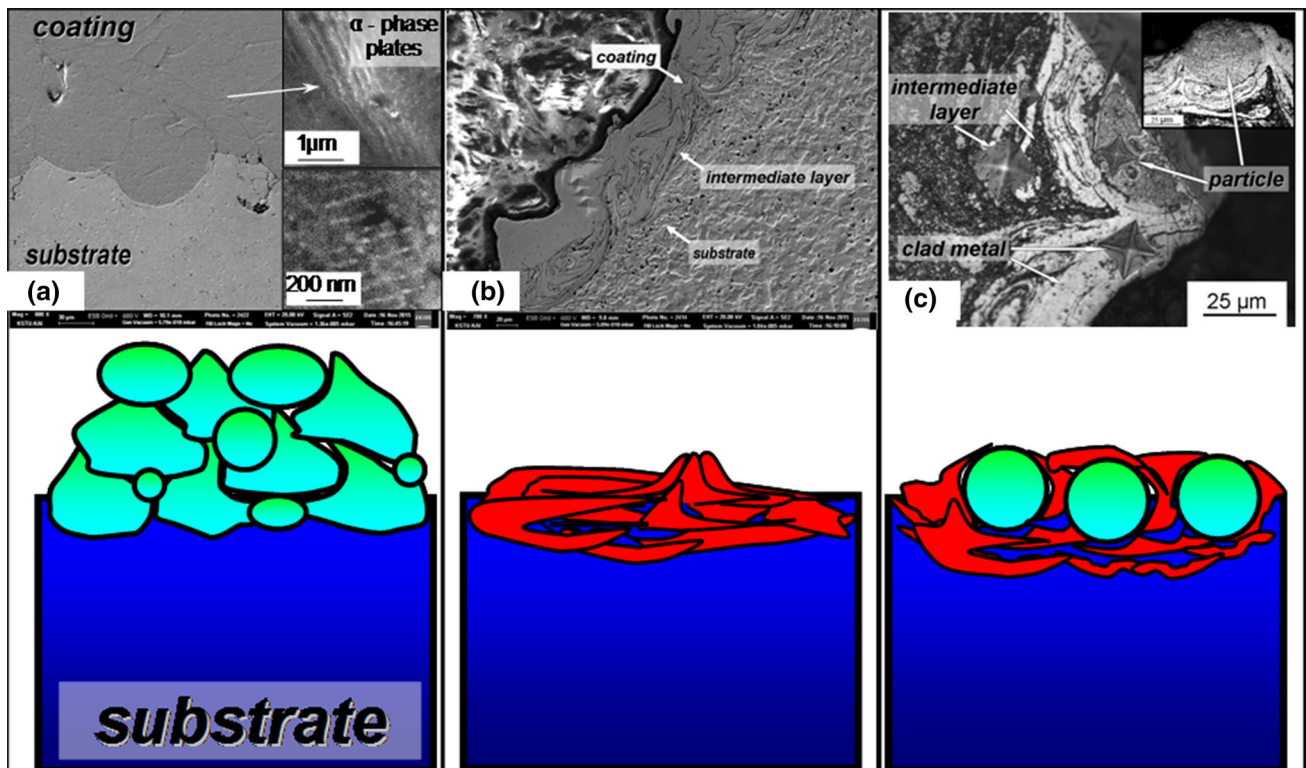
### Main Types of Coatings Obtained by Supersonic Laser Deposition

Figure 2 shows the types of the coatings obtained by SLD and their respective schematic representations.

As shown in Fig. 2(a), the titanium-based coating is formed without melting of the powder material; the structure and the properties of the initial powder material remain. Figure 2(b) illustrates the melting of the powder material and the formation of the coating containing the particles of the same powder material. The inclination angle of the laser was adjusted to coincide with the laser spot and the powder material. The resulting structures are shown in Fig. 2(b) and (c).

Thus, the SLD coatings can be divided into the following groups: the coatings obtained without melting of the powder material, the coatings obtained with complete melting of the powder material, and the coatings applied with partial melting and subsequent embedding of the particles.

Such a classification is proposed on the basis of the experimental results for both soft and hard coatings. In the past, in the absence of the laser irradiation, the classic cold spray process allowed the creation of the coatings without melting of the powder material, which significantly limited the range of possible substrates.



**Fig. 2** Basic types of coatings applied by supersonic laser deposition without melting the powder material TA15 (a), with complete melting of the powder material, NiCrCBSiFe (b), and with melting of the coating and subsequent embedding of the powder particles of NiCrCBSiFe (c)

Figure 2(c) shows that the powder particles that are embedded in the surface of the coating and in the substrate have a shape close to a drop. Particles found in the coating cross-section have various shapes. For example, if the temperature of the solid–liquid phase is in the range of 600–700 °C, the particles can retain their spherical shape and penetrate into the substrate surface. However, if the temperature range of the coating surface is 750–800 °C, the particles have the shape of a drop. In this case, the particles overcome the surface tension forces of the melt and transform. There are layers of deposited metal that are resistant to chemical etching while the area around is perfectly etchable.

If the temperature of the molten metal on the coating surface is in the range of 450–500 °C, the solid NiCrBSi-FeC particles that impinge on the coating surface do not penetrate into the surface but deform and compact it. In this case, striations obtained by the deformation of the coating metal may be observed in the sample cross-section. It may be assumed that this type of the treatment increases the density of the coating, reduces the number of dislocations and increases the hardening effect.

When spraying, the powder particle speed reaches 700 m/s, thereby providing a higher strength and density of the coating. However, the speed of more than 700 m/s

leads to the sputtering of the molten particles and the coating degradation.

There are certain difficulties arising from the application of the supersonic nozzles, which are attributed to the powder particles sticking to the walls of the nozzle. It is inefficient to inject the powder into the supersonic jet at the outlet due to a sharp reduction of the acceleration section and the discontinuity of the powder jet. Therefore, there is a contradiction: on the one hand, it is efficient to feed the powder into the gas ahead of the critical section, but on the other hand it is necessary to avoid possible collisions of the accelerated liquid particles with the walls of the channel over its entire length. The carrier gas temperature must not exceed 550 °C to avoid the sticking of NiCrCBSiFe particles to the inner walls of the nozzle.

### Elemental Analysis of the Coatings

In Fig. 3(b), it can be seen that the interval with a sudden change on the histogram is rather short. This is primarily related to the fact that the coating has been plastically deformed by the solid particles. As a result, chemical heterogeneity can be observed.

Figure 4 shows the distribution of the basic elements in the coating metal and the substrate metal.

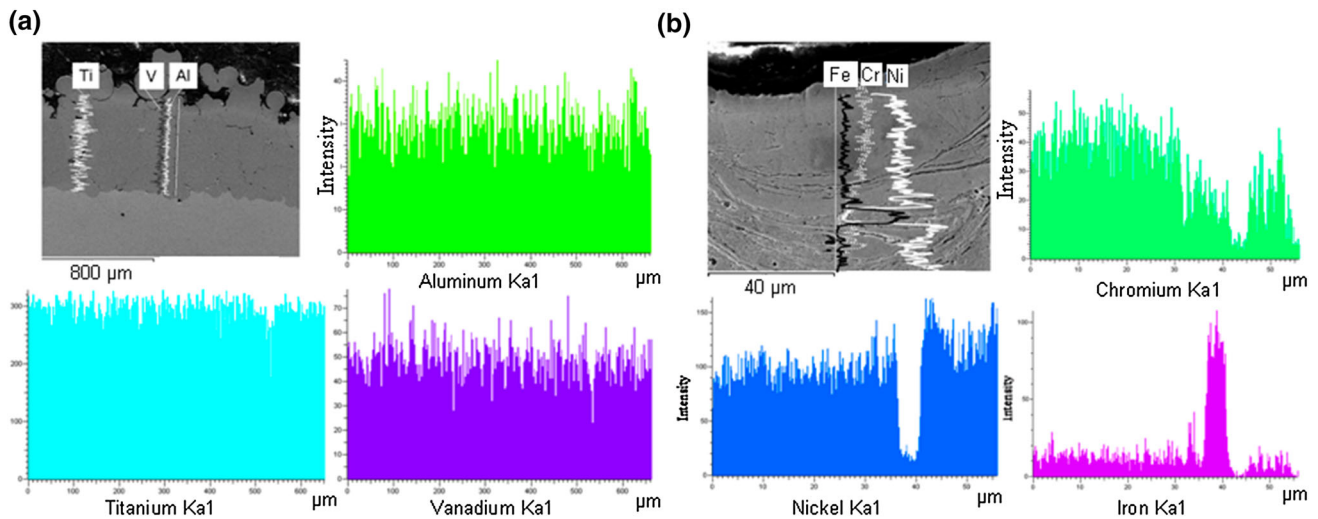


**Fig. 3** Chemical elements distribution in the cross-section of coatings based on Ti (a) and NiCrCBSiFe (b)

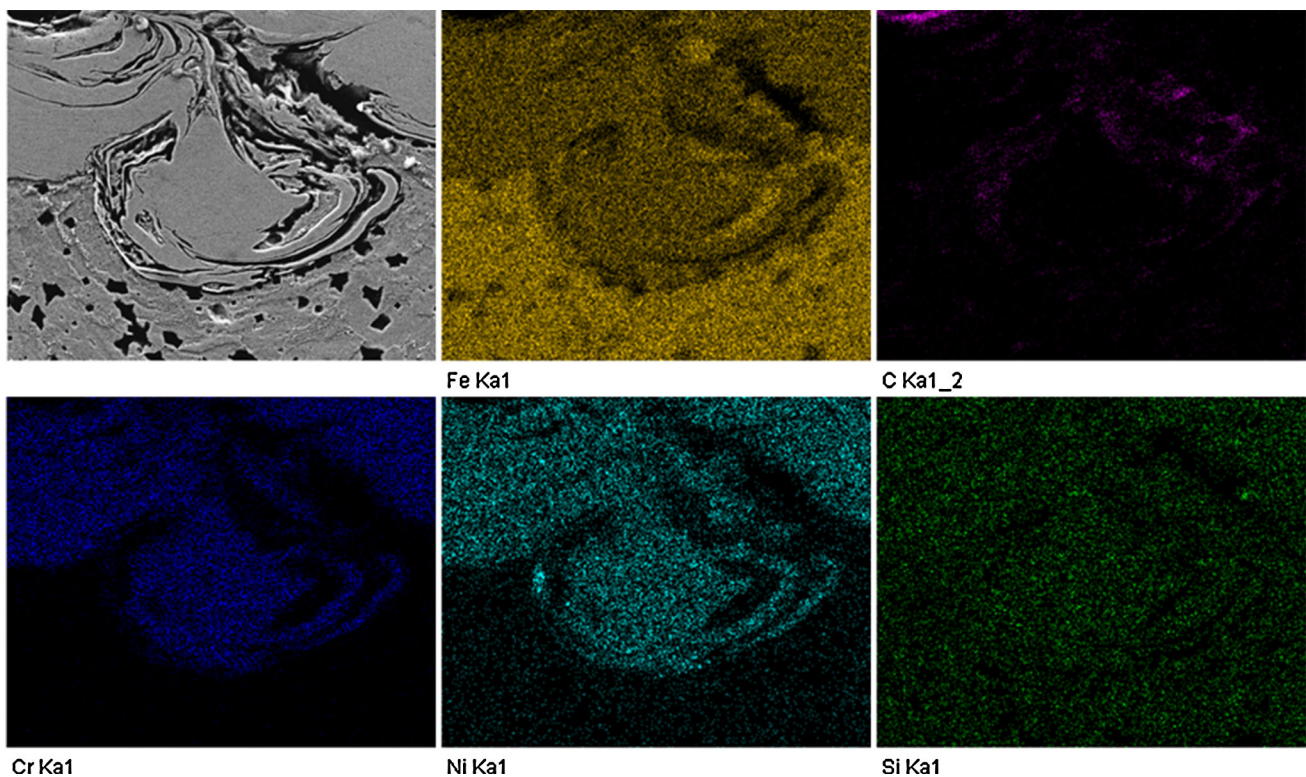


**Fig. 4** Mapping in the region of NiCrCBSiFe particles embedded into the coating and the steel substrate

When the particles are embedded in the coating and the substrate, a nickel band around the NiCrCBSiFe particles appears, and it can be seen that there is iron between the nickel bands around the particles. The mapping shows a unique picture: when the powder particles move through the coating before becoming embedded in the base metal of the substrate, and the metal of the particle mixes partly with the substrate metal. Due to the different densities and the short period of time when the

base metal and the coating remain liquid, complete mixing or dissolution of the melts is not observed. As for the remaining elements, for example, silicon and carbon, there is no any significant contrast in comparison with iron and nickel, because these elements are present both in the coating and in the substrate, and their percentage ratio is almost the same. However, elements such as chromium, which has a negligible weight ratio compared to its content in the substrate, do not dissolve or diffuse. It

repeats the contour of the particle and the parts that became separated from it.

### Analysis of the Phase Composition of Coatings

Spraying of the TA15 titanium alloy made it possible to obtain a coating with the same phase composition as the original powder material, so that there are no peaks of primed or double-primed alpha on the diffraction pattern (Fig. 5a). This suggests that during spraying the metastable state represented by martensitic phase has not been achieved; furthermore, it will have a positive effect on the mechanical properties.

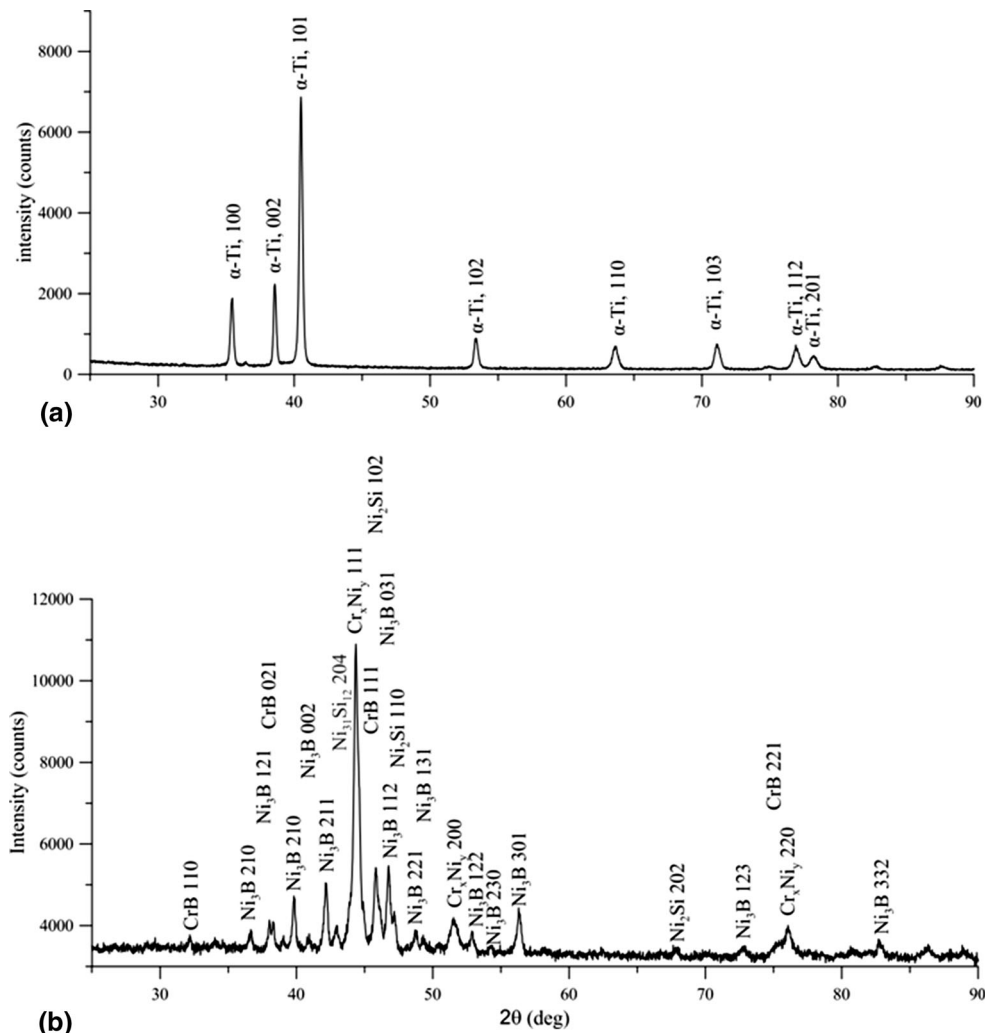
The laser power density and the cooling rate play an important role when obtaining the coating followed by the melting of the powder material. In this case, when laser-assisted melting takes place, the following phases are formed (Fig. 5b). Melting of the NiCrCBSiFe metallic powder leads to the formation of a large number of phases of the same type with different values of the stoichiometric

coefficients (Fig. 5b). The phase composition of the particles embedded in the coating remains the same. It is known that the formation of the phases with the corresponding stoichiometric coefficients depends to a great extent on the energy source. It can be seen in the literature that the plasma-assisted melting of the powder material with the composition of the NiCrCBSiFe system leads to the formation of Cr<sub>3</sub>Ni<sub>2</sub>SiC, Cr<sub>23</sub>C<sub>6</sub>, Cr<sub>7</sub>BC<sub>4</sub>, (FeNi)<sub>23</sub>C<sub>6</sub>, Fe<sub>3</sub>C, Ni<sub>3</sub>B, and SiC, respectively Ref (28).

In this case, when the spraying process is intensified by a fiber laser, the XRD analysis of the sample (Fig. 5b) reveals the following phases:

1. FCC-phase of the matrix, which can be described by a number of Cr<sub>x</sub>Ni<sub>y</sub> phases (Cr<sub>0.1</sub>Ni<sub>0.9</sub> ICDD PDF-2 01-074-5730, Cr<sub>1.12</sub>Ni<sub>2.88</sub> ICDD PDF-2 03-065-5559). The matrix is a nickel FCC-lattice (ICDD PDF-2 01-071-4653) with doping impurities.
2. Ni<sub>3</sub>B (ICDD PDF-2 01-072-9062, 00-048-1223).
3. CrB (ICDD PDF-2 03-065-0413).

**Fig. 5** XRD patterns of the samples: sprayed TA15 (a) and NiCrCBSiFe (b) coatings in the range of 2θ 25-90°



4.  $\text{Ni}_2\text{Si}$  nickel silicides (ICDD PDF-2 01-072-2547) and, presumably,  $\text{Ni}_{31}\text{Si}_{12}$  (ICDD PDF-2 00-017-0222).

The phase analysis presented in Fig. 6 shows that the amount of the iron–nickel phases in the  $\text{Fe}_x\text{Ni}$  111- and  $\text{Fe}_x\text{Ni}$  200-based coatings gradually decreases and completely disappears in the metal through-thickness. Figure 6(a) confirms that the substrate metal and the metal of the NiCrBSiFeC coating are mixed (see the content of  $\alpha\text{-Fe}$  110). Estimation of the mixing degree of the base substrate metal with the coating metal by the relative change in the  $\alpha\text{-Fe}$  110 phase aroused interest, in this case, it was  $\approx 21\%$ .

When studying the diffraction patterns indicated by red lines in different coating cross-sections shown in Fig. 6(b), formation of new additional phases—combinations of nickel (which is a part of the coating) with iron (which is a part of the substrate) is observed in through-thickness from the coating to the substrate.

The diffraction pattern of Fig. 6 shows the diffraction peaks of  $\alpha\text{-Fe}$  (ICDD PDF-2 00-006-0696), Ni (ICDD PDF-2 01-071-4653), and  $\text{Fe}_x\text{Ni}_y$  (a number of phases of  $\text{Fe}_{0.64}\text{Ni}_{0.36}$  -ICDD PDF-2 00 -047-1405,  $\text{Fe}_3\text{Ni}$  - ICDD

PDF-2 03-065-5131,  $\text{FeNi}$  - ICDD PDF-2 01-077-7974, etc.).

This gives an idea that additional phases can cause a certain decrease in the hardness of the coating matrix relative to the embedded powder material. Such a combination of a soft matrix and embedded solid particles will make it possible to avoid cracking, as happens with NiCrBSiFe coatings in the case of classical cladding because of the large internal stresses.

During the NiCrBSiFe coating production, a molten pool can be formed in both the classical LC and the SLD. In the case of the classical cladding; the energy of the particles is not enough to overcome the surface tension forces, and the particles rebound. In the case of SLD, the particles gain the speed sufficient to overcome the surface tension forces, and they penetrate into the inner layers of the molten metal.

However, it should be taken into account that the shape of the particles in the coating depends on the impact with the substrate. Different combinations of the structure and the hardness can be obtained by varying the mixing degree of the deposited metal with the substrate metal. Of course,

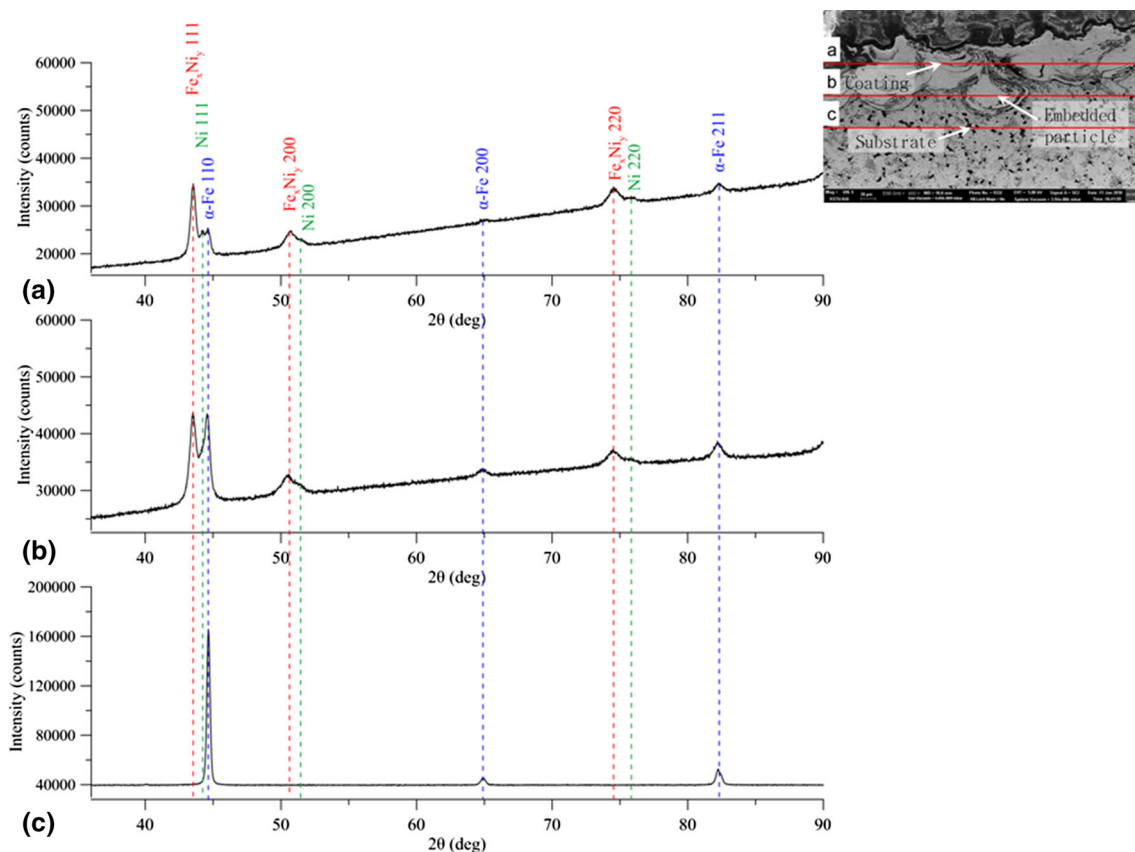


**Fig. 6** Diffraction patterns of the sample with NiCrBSiFe coating in the range of  $2\theta$  36–90°, obtained from different areas of analysis (a, coating (cladding layer), b, transition range, c, the substrate area) (Color figure online)

the higher the mixing degree, the greater the molten pool, and the softer the solid–liquid region, and the easier it is for the particles to overcome the surface tension forces and penetrate deep into the metal. However, at a certain ratio, such a combination can cause metal spatter and damage the coating’s integrity.

**Analysis of the Structure of the Substrate and the Regions Adjacent to the Coating**

For a more detailed study of the embedded particle and the adjacent metal, deep etching was carried out. The results are presented in Fig. 7 and 8.

It can be seen in Fig. 7(a) that the particles pass through the coating and make a mix of the molten metal of the coating and the substrate metal. In this case, the particles do not collide with the substrate. The particles are gently immersed in the coating. The edges of the particles may be partially decompressed. In this case, the powder particles have the shape of a drop. The particles go deep and remain both in the nickel-based coating formed by the same melted particles, and in the metal of the steel substrate.

The coating was obtained at 50% overlap of the laser spot focus and the gas powder flow spot. Mixing of the

substrate metal with the deposited material leads to a 9% increase in hardness. The hardness of the embedded particles is 18% greater than that of the deposited metal (Fig. 7b). However, the addition of the  $\alpha$ -Fe 110 phase in the amount of 21% to the molten NiCrBSiFeC coating results in an 18% loss of hardness compared to the initial powder material.

The cooling rate of the melt is less than the critical cooling rate. Therefore, during the decay of austenite, we obtain a ferrite–cementite mixture, perlite. Figure 8 shows the structure of the base metal of the areas adjacent to the coating metal and the nickel-based embedded particles.

A stable perlite structure is more preferable than a metastable martensitic structure, which is achievable at high cooling rates. The cooling of the substrate metal is slow because the crystallization of the steel and the formation of austenite grains begin at the temperature of 1539 °C. On the other hand, boron and silicon form low-melting eutectics with nickel with a melting point of 950–1080 °C in the coating metal, and also reduce the oxide films on the surface of the substrate to form borosilicate slags (self-fluxing) in the presence of the liquid phase. They improve the wettability of the substrate by the liquid metal. This implies that the cooling starts at the

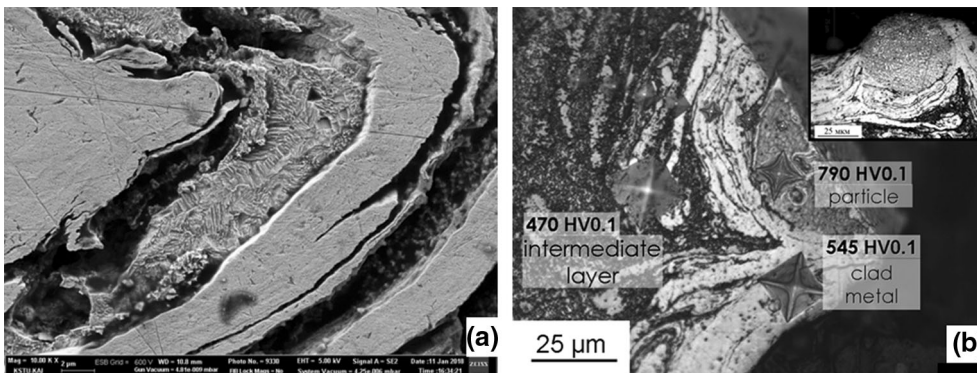


**Fig. 7** Microphotography of the boundary between the metal of the substrate and the embedded NiCrBSiFe particle (a), measuring the microhardness of a particle and metal regions adjacent to it (b)

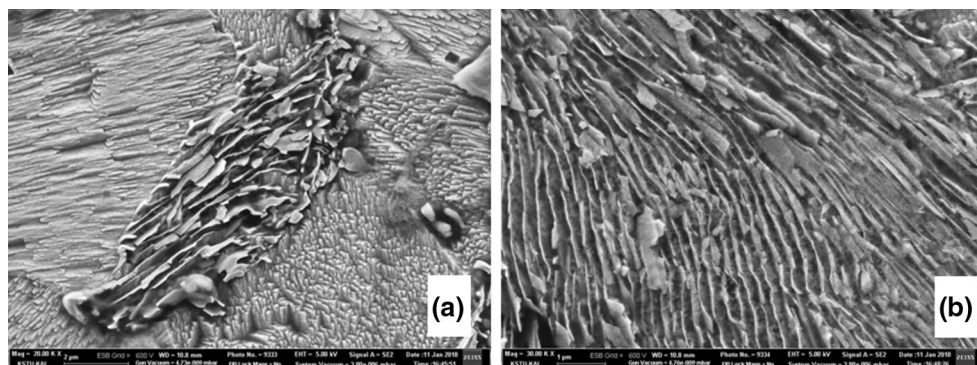


**Fig. 8** The pearlite structure of the substrate metal adjacent to the coating based on NiCrBSiFe



surface of the substrate. However, liquid areas on the coating provide a possibility of a gradual cooling after the coating is applied. Presumably, the residual stresses will be small due to the gradual cooling of the coating. Therefore, annealing in this case is not required.

Supersonic impingement of the powder particles on the molten coating and further embedding provide a possibility to retain, partly control, and initially tailor the structure and the properties of the coating, as well as to create wear-resistant coatings with a low melting point.

## Conclusions

Earlier studies have shown that LC and cold spray provide unique opportunities for both coating and additive production. Combining the qualities of both processes, SLD opens up unique opportunities for obtaining new materials. The SLD method allows three modes of coating production (without melting, with melting and partial melting of powder particles and embedding of the particles into the coating). In this work, a fiber laser was chosen as the additional source of energy in the cold spray process, but a CO<sub>2</sub> laser or induction heating could also have been used.

However, remaining questions are whether it is possible to obtain grading coatings with the SLD process, for example, by alternating coatings deposited without melted and with melted particles, and what would be the mechanical properties of such coatings. These questions will be answered in the coming months.

**Acknowledgment** The author acknowledges support from the Ministry of Education of the Russian Federation for supporting the research Project No 9.3236.2017/4.6.

## References

1. A.P. Alkhimov, S.V. Klinkon, V.F. Kosarev, and A.N. Papyrin, Gasdynamicspraying. Study Plane Supersonic Two-Phase Jet, *J. Appl. Mech. Tech. Phys.*, 1977, **38**(2), p 177
2. F. Luo, A. Cockburn, D. Cai, M. Sparkes, Y. Lu, C. Ding, R. Langford, W. O'Neill, J. Yao, and R. Liu, Simulation Analysis of Stellite 6<sup>®</sup> Particle Impact on Steel Substrate in Supersonic Laser Deposition Process, *J. Therm. Spray Technol.*, 2015, **24**(3), p 378-393
3. F. Luo, A. Cockburn, R. Lupoi, M. Sparkes, and W. O'Neill, Performance Comparison of Stellite 6 Deposited on Steel Using Supersonic Laser Deposition and Laser Cladding, *Surf. Coat. Technol.*, 2012, **212**, p 119-127
4. F. Luo, R. Lupoi, A. Cockburn, M. Sparkes, and W. O'Neill, Characteristics of Stellite 6 Deposited by Supersonic Laser Deposition Under Optimized Parameters, *J. Iron. Steel Res. Int.*, 2013, **20**(2), p 52-57
5. J. Yao, Z. Li, B. Li, L. Yang, and J. Yaoet, Characteristics and Bonding Behavior of Stellite 6 Alloy Coating Processed with Supersonic Laser Deposition, *J. Alloys Compd.*, 2016, **661**, p 526-534
6. H. Ren, X. Tian, D. Liu, J. Liu, and H. Wang, Microstructural Evolution and Mechanical Properties of Laser Melting Deposited Ti-6.5Al-3.5Mo-1.5Zr-0.3Si Titanium Alloy, *Trans. Nonferrous Met. Soc. China*, 2015, **25**, p 1856-1864
7. R.E. Blöse, B.H. Walker, R.M. Walker, and S.H. Froes, New Opportunities to Use Cold Spray Process for Applying Additive Features to Titanium Alloys, *Powder Rep.*, 2006, **61**, p 30-37
8. S.H. Zahiri, C.L. Antonio, and M. Jahedi, Elimination of Porosity in Directly Fabricated Titanium Via Cold Gas Dynamic Spraying, *J. Mater. Process. Technol.*, 2009, **209**, p 922-929
9. D. Goldbaum, J. Ajaja, R.R. Chromik, W. Wong, S. Yue, E. Irissou, and J.-G. Legoux, Mechanical Behavior of Ti Cold Spray Coatings Determined By a Multi-Scale Indentation Method, *Mater. Sci. Eng. A*, 2011, **530**, p 253-265
10. R.S. Lima, A. Kucuk, C.C. Berndt, J. Karthikeyan, C.M. Kay, and J. Lindeman, Deposition Efficiency, Mechanical Properties and Coating Roughness in Cold-Sprayed Titanium, *J. Mater. Sci. Lett.*, 2002, **21**, p 1687-1689
11. T. Marrocco, D.G. McCartney, P.H. Shipway, and A.J. Sturgeon, Production of Titanium Deposits by Cold-Gas Dynamic Spray: Numerical Modeling and Experimental Characterization, *J. Therm. Spray Technol.*, 2006, **15**, p 263-272
12. S. Grigoriev, A. Okunkova, A. Sova, P. Bertrand, and I. Smurov, Cold Spraying: From Process Fundamentals Towards Advanced Applications, *Surf. Coat. Technol.*, 2015, **268**, p 77-84
13. M. Tewolde, G. Fu, D.J. Hwang, L. Zuo, S. Sampath, and J.P. Longtin, Thermoelectric Device Fabrication Using Thermal Spray and Laser Micromachining, *J. Therm. Spray Technol.*, 2016, **25**(3), p 431-440
14. R.C. Seshadri, G. Dwivedi, V. Viswanathan, and S. Sampath, Characterizing Suspension Plasma Spray Coating Formation Dynamics through Curvature Measurements, *J. Therm. Spray Technol.*, 2016, **25**(8), p 1666-1683
15. R. Lupoi, M. Sparkes, A. Cockburn, and W. O'Neill, High Speed Titanium Coatings by Supersonic Laser Deposition, *Mater. Lett.*, 2011, **65**, p 3205-3207
16. N. Bala, H. Singh, and S. Prakash, Performance of Cold Sprayed Ni Based Coatings in Actual Boiler Environment, *Surf. Coat. Technol.*, 2017, **318**(25), p 50-61
17. W. Sun, A.W.Y. Tan, N.W. Khun, I. Marinescu, and E. Liua, Effect of Substrate Surface Condition on Fatigue Behavior of Cold Sprayed Ti6Al4V Coatings, *Surf. Coat. Technol.*, 2017, **320**(25), p 452-457
18. R. Singh, K.-H. Rauwald, E. Wessel, G. Mauer, S. Schrufer, A. Barthd, S. Wilson, and R. Vassena, Effects of Substrate Roughness and Spray-Angle on Deposition Behavior of Cold-Sprayed Inconel 718, *Surf. Coat. Technol.*, 2017, **319**, p 249-259
19. F. Luo, A. Cockburn, M. Sparkes, R. Lupoi, Z. Chen, W. O'Neill, J. Yao, and R. Liu, Performance Characterization of Ni60-WC Coating on Steel Processed with Supersonic Laser Deposition, *Def. Technol.*, 2015, **11**, p 35-47
20. Y. Zhou, G. Ma, and H. Wang, Microstructures and Tribological Properties of Fe-Based Amorphous Metallic Coatings Deposited via Supersonic Plasma Spraying, *J. Therm. Spray Technol.*, 2017, **26**(6), p 1257-1267
21. A.I. Gorunov and A.K. Gilmudtinov, Investigation of Coatings of Austenitic Steels Produced by Supersonic Laser Deposition, *Opt. Laser Technol.*, 2017, **88**, p 157-165
22. J.H. Yao, L.J. Yang, B. Li, Q.L. Zhang, and Z.H. Li, Deposition Characteristics and Microstructure of a Ni60-Ni Composite Coating Produced by Supersonic Laser Deposition, *Lasers Eng.*, 2017, **36**(1-3), p 117-131
23. J. Yao, L. Yang, B. Li, Z. Li, and J. Yaoet, Characteristics and Performance of Hard Ni60 Alloy Coating Produced with

- Supersonic Laser Deposition Technique, *Mater. Design*, 2015, **83**, p 26-35
24. L. Yang, B. Li, J. Yao, Z. Li, and L. Yanget, Effects of Diamond Size on the Deposition Characteristic and Tribological Behavior of Diamond/Ni60 Composite Coating Prepared By Supersonic Laser Deposition, *Diam. Relat. Mater.*, 2015, **58**, p 139-148
25. B. Li, J. Yao, Q. Zhang, Z. Li, and L. Yanget, Microstructure and Tribological Performance of Tungsten Carbide Reinforced Stainless Steel Composite Coatings By Supersonic Laser Deposition, *Surf. Coat. Technol.*, 2015, **275**, p 58-68
26. L. Yuan, F. Luo, J. Yao, L. Yuan, and F. Luo, Deposition Behavior At Different Substrate Temperatures by Using Supersonic Laser Deposition, *J. Iron Steel Res. Int.*, 2013, **20**(10), p 87-93
27. M. Jones, A. Cockburn, R. Lupoi, M. Sparkes, and W. O'Neill, Solid-State Manufacturing of Tungsten Deposits Onto Molybdenum Substrates with Supersonic Laser Deposition, *Mater. Lett.*, 2014, **134**, p 295-297
28. V.I. Kalita, V.V. Yarkin, V.P. Bagmutov, S.N. Parshev, I.N. Zakharov, A.V. Kasimtsev, G.U. Lubman, D.I. Komlev, and V.I. Mamonov, Formation of Coatings with Nanostructures and Amorphous Structures, *Russ. Metall. (Metally)*, 2007, **2007**(6), p 534-539